Supplementary Materials

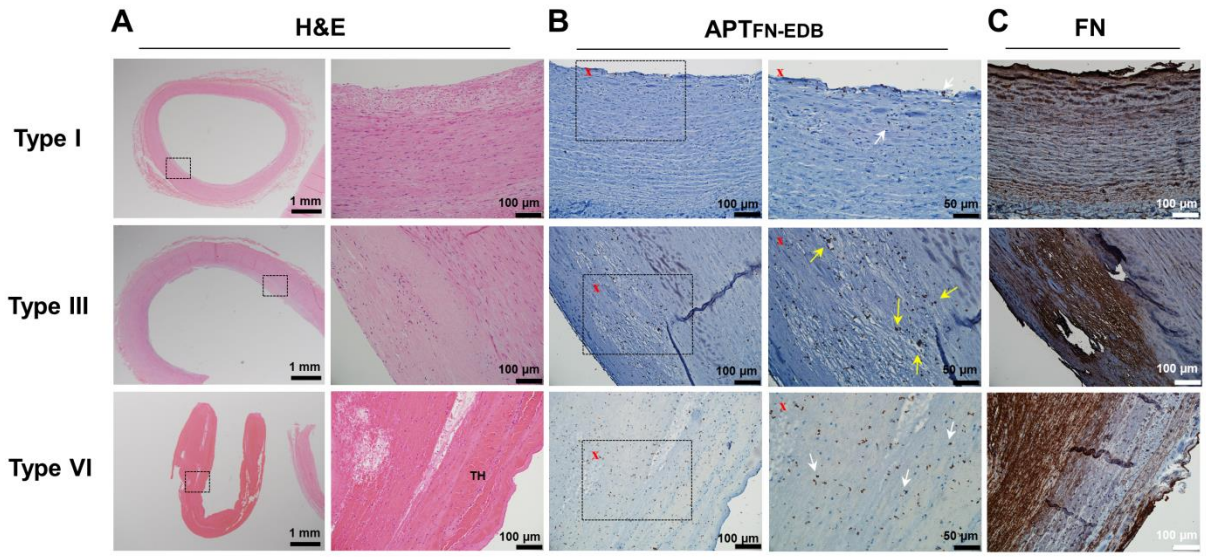

Figure S1. Representative photomicrographs of atherosclerotic lesions of type I, type III, and type VI stained with H&E or $APT_{FN\text{-}EDB}$ (for FN-EDB), or for FN. **(A)** Left: Low-magnification images of H&E-stained sections. Scale bar = 1 mm. Right: Magnified views corresponding to the black rectangles in adjacent H&E images. Scale bars = 100 μm. **(B)** Left: Low-magnification images of $APT_{FN\text{-}EDB}$ staining results. Scale bar = 100 μm. Right: Magnified views corresponding to the black rectangles in adjacent image labeled with an "x". Scale bar = 50 μm. Arrows, FN-EDB–positive areas. **(C)** FN staining results. Scale bar = 100 μm. TH, thrombus.

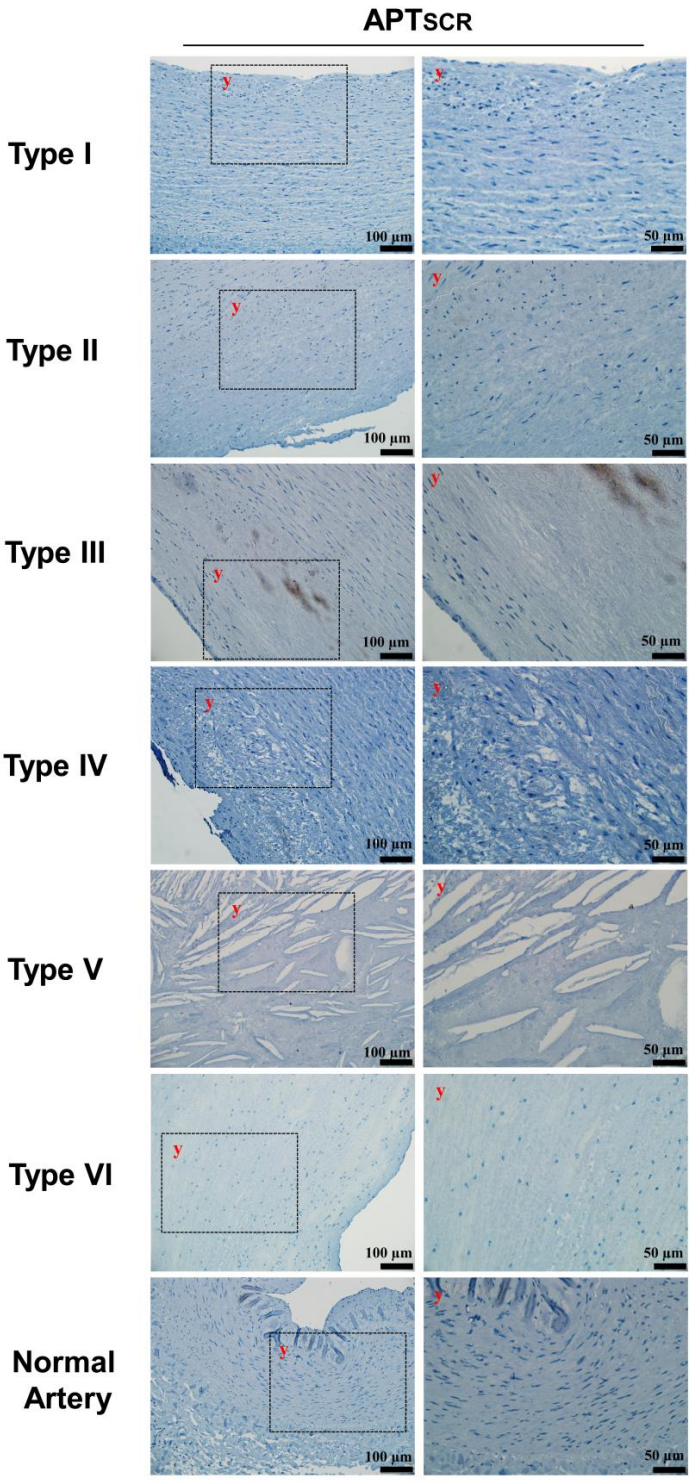

Figure S2. FN-EDB–positive areas stained with $APT_{FN\text{-}EDB}$ were compared with the corresponding areas stained with APT_{SCR} (negative control). Left: Low-power image. Scale bar = 100 μm. Right: Magnified images of black rectangles labeled 'y' in adjacent images. Scale bar = 50 μm.

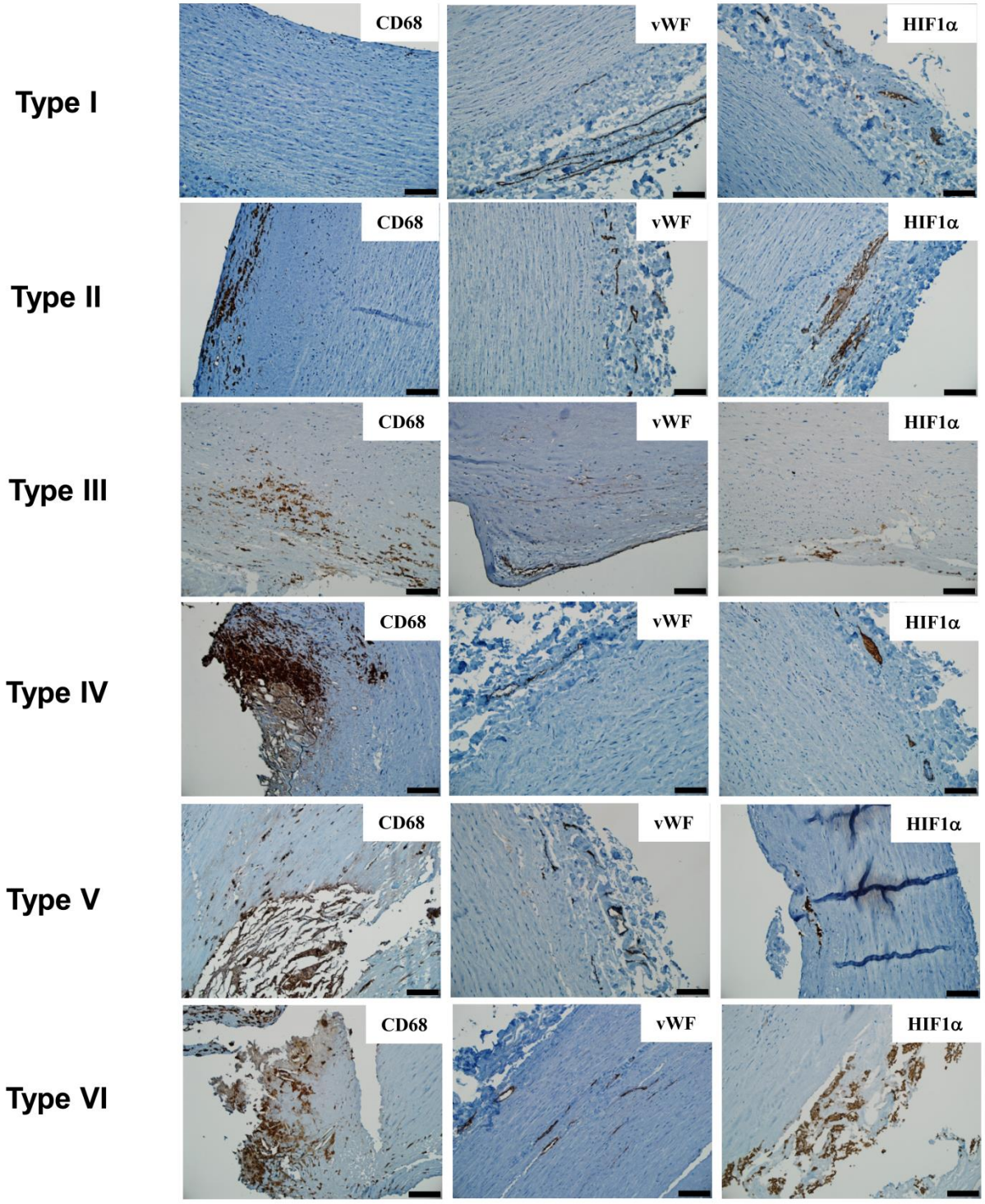

Figure S3. Representative images of atherosclerotic lesions from type I–VI lesions analyzed for FN-EDB were stained for CD68, vWF, or HIF1α. Scale bar = 100 μm.

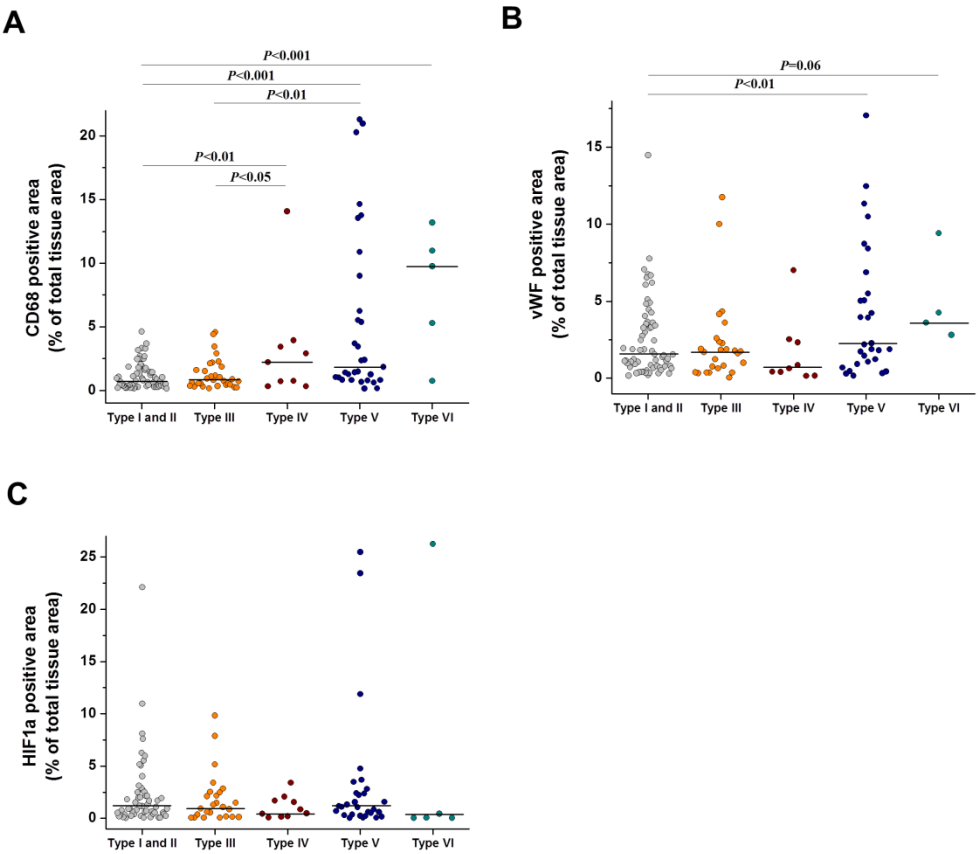

Figure S4. (A-C) Quantitative assessment of areas positive for CD68, vWF, or HIF1α in different types of human atherosclerotic lesions. (Type I and II, *n* = 71; type III, *n* = 30; type IV, *n* = 9; type V, *n* = 32; type VI, *n* = 5). Data are for individual tissue sections; means are shown as horizontal lines.

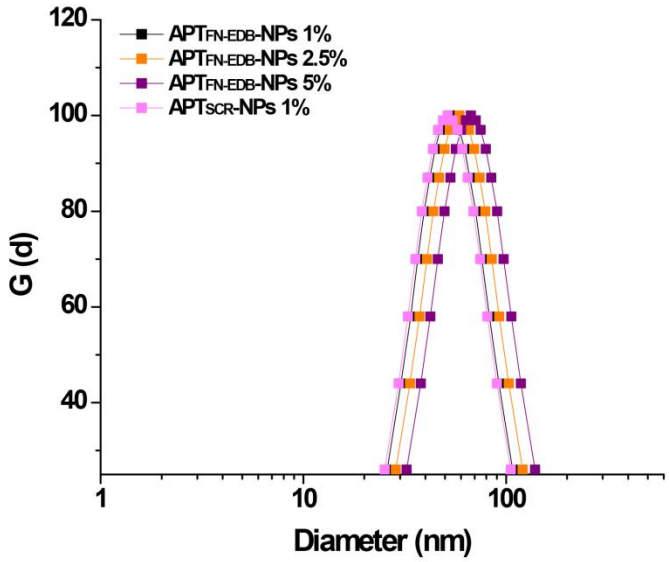

Figure S5. $APT_{FN\text{-}EDB}$-NPs and APT_{SCR}-NPs with different densities of $APT_{FN\text{-}EDB}$ and APT_{SCR}, respectively, were prepared and their hydrodynamic sizes measured by DLS.

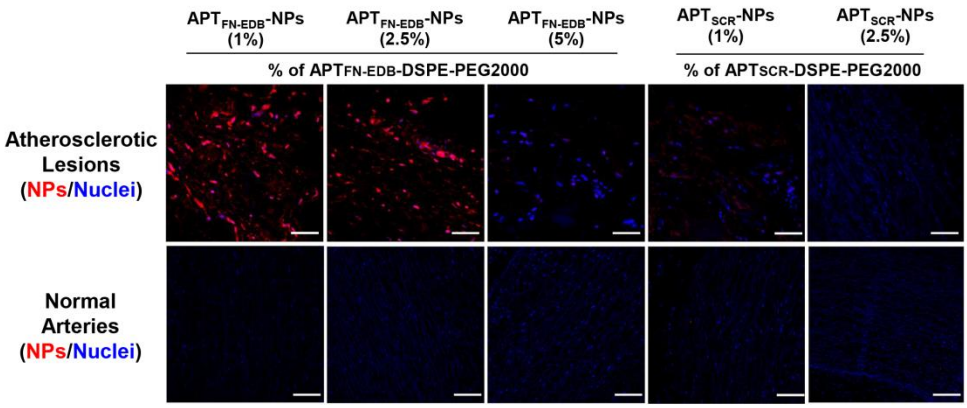

Figure S6. Atherosclerotic lesion detection efficiencies by NPs (*red*) and comparison with normal arteries. Confocal microscopic images show that human atherosclerotic lesions are effectively detected by $APT_{FN\text{-}EDB}$-NPs (1% or 2.5% molar ratios of $APT_{FN\text{-}EDB}$-DSPE-PEG2000). In contrast, binding of $APT_{FN\text{-}EDB}$-NPs (5% molar ratio of $APT_{FN\text{-}EDB}$-DSPE-PEG2000) and APT_{SCR}-NPs (1% or 2.5% molar ratio of APT_{SCR}-DSPE-PEG2000) with atherosclerotic lesions and binding of NPs with normal arteries are negligible. Scale bar = 60 μm.

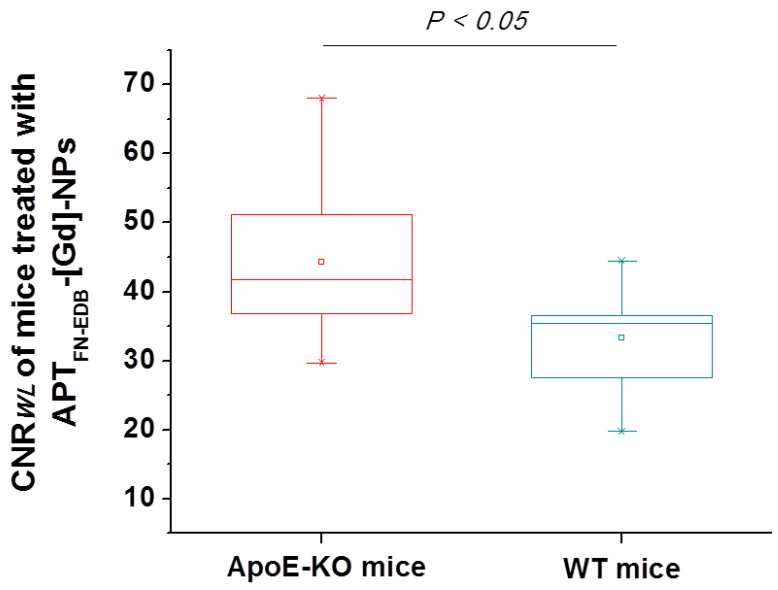

Figure S7. *In vivo* MRI of $APT_{FN\text{-}EDB}$-[Gd]NPs in hypercholesterolemic apoE-KO mice and in WT mice (C57BL/6J) on a normal chow diet. CNR_{WL} values of apoE-KO mice on a 16-wk WD treated with $APT_{FN\text{-}EDB}$-[Gd]NPs (n = 15) were compared with those of WT mice treated with $APT_{FN\text{-}EDB}$-[Gd]NPs (n = 6).

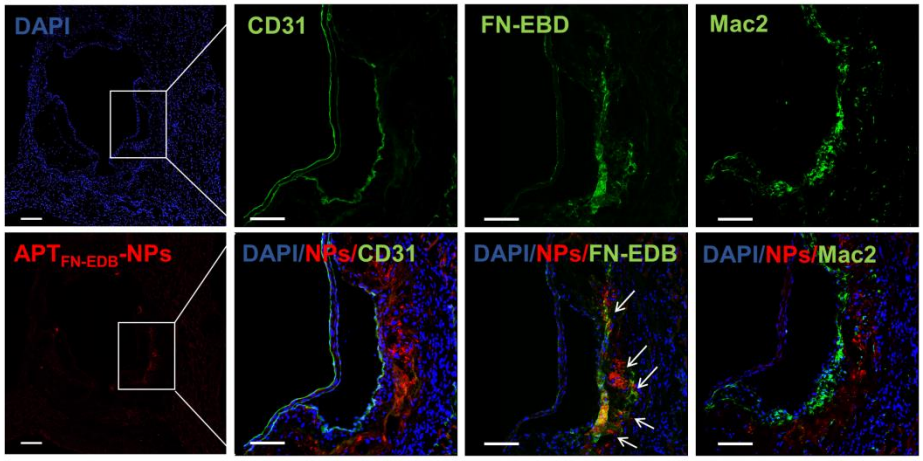

Figure S8. FN-EDB mediated plaque accumulation of $APT_{FN\text{-}EDB}$-NPs. Immunofluorescent staining of endothelial cells (CD31), FN-EDB, and macrophages (Mac2) in the atherosclerotic plaques of apoE-KO mice (n=4) injected with $APT_{FN\text{-}EDB}$-NPs revealed that plaque accumulation of the NPs was mainly co-localized with FN-EDB expression (*arrows*) rather than with endothelial cell or macrophage expression. Left: 6x magnification of aortic root. Visualization of nuclei (*upper image*) and $APT_{FN\text{-}EDB}$-NPs (*lower image*). Right: 20x magnification of aortic roots show immunofluorescent staining of CD31, FN-EDB, and Mac2 (*green*, *upper images*), or merged images with $APT_{FN\text{-}EDB}$-NPs (*red*) and nuclei (*blue*) (*lower images*). Scale bar = 80 µm.

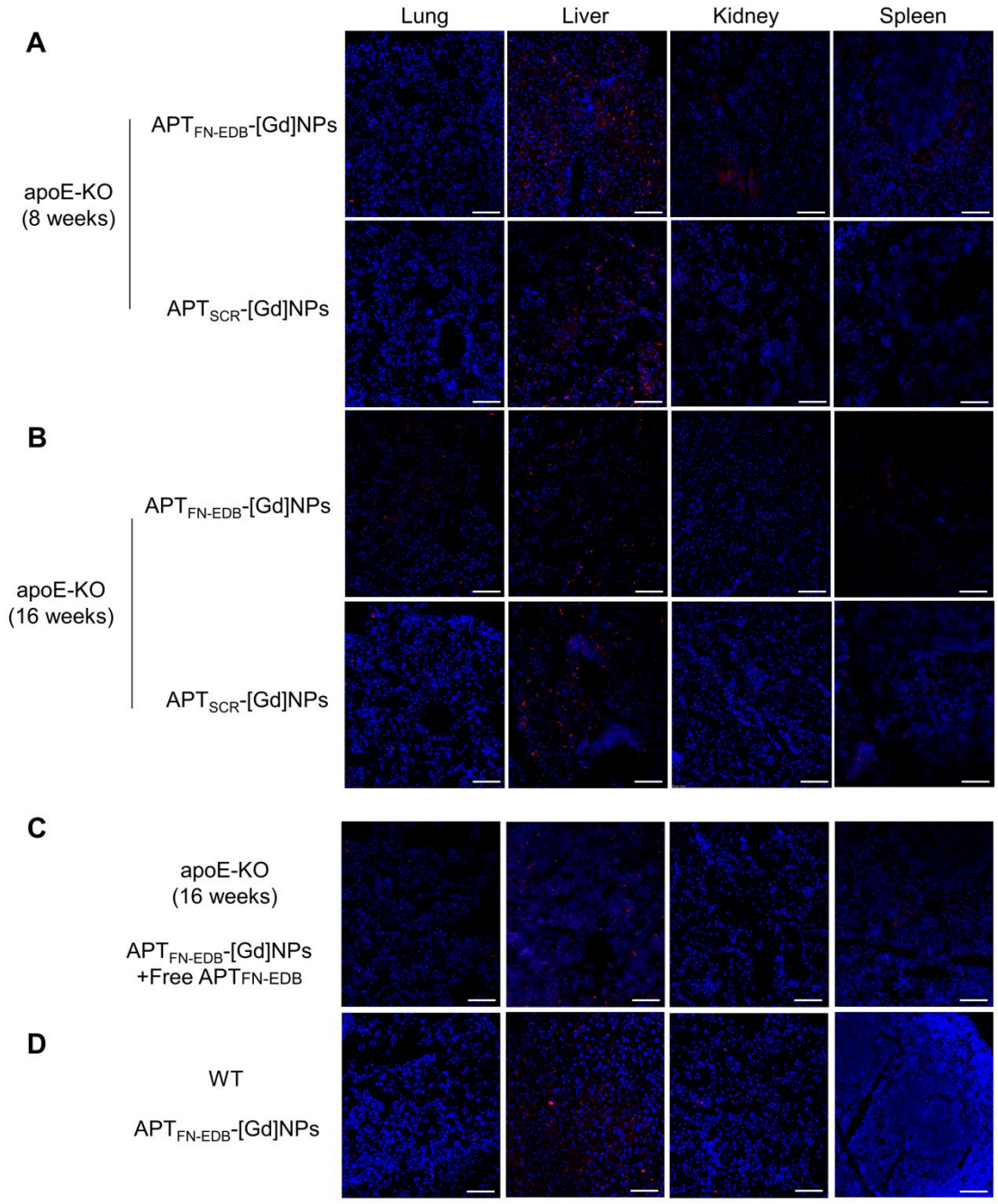

Figure S9. *In vivo* biodistribution of $APT_{FN\text{-}EDB}$-[Gd]NPs and APT_{SCR}-[Gd]NPs. Confocal microscopic images of DAPI-stained lung, liver, kidney, and spleen sections showing NPs (*red*) and nuclei (*blue*) in apoE-KO mice consumed a WD for (**A)** 8 wk or (**B)** 16 wk. (**C-D)** Comparison of corresponding organs from apoE-KO mice (consumed a WD for 16 wk) pre-injected with free $APT_{FN\text{-}EDB}$ prior to $APT_{FN\text{-}EDB}$-[Gd]NPs injection and WT mice injected with $APT_{FN\text{-}EDB}$-[Gd]NPs. Scale bar = 60 µm.